COMMUNICATIONS
FROM THE
KONKOLY OBSERVATORY
OF THE
HUNGARIAN ACADEMY OF SCIENCES

MITTEILUNGEN
DER
STERNWARTE
DER UNGARISCHEN AKADEMIE
DER WISSENSCHAFTEN

BUDAPEST — SZABADSÁGHEGY

No. 95.
(Vol. 11, Part 2)

DISTRIBUTION OF LATE-TYPE STARS AROUND IC 4665

A FRONTÓ, L. G. BALÁZS, M. PAPARÓ

BUDAPEST, 1989

ISBN 963 8361 33 6
HU ISSN 0238 — 2091

Felelős kiadó: Szeidl Béla

Hozott anyagról sokszorosítva

9119739 **AKADRINT Nyomdaipari Kft. Budapest. F. v.: dr. Héczey Lászlóné**

Distribution of Late-Type Stars Around IC 4665

ABSTRACT

We have investigated 424 stars of F8 spectral types and later in a 19.5 sq. degree field around IC 4665. The main purpose of our study in this low latitude field (b=+16.5 in our case) was the testing of the plane-parallel hypothesis of the density distribution, i.e. the hypothesis that the spatial density of the Population I stars observed at great angular distance from the galactic caps is well approximated by the z = r sin(b) scaling of the distributions obtained in the polar regions.

We used the factor analysis of multivariate mathematical statistics in order to extract the effect of absorption from the photometric data. To identify the factor component describing the interstellar reddening we invoked the corresponding IRAS Sky Flux Data. We computed the spatial densities for the F8 - G5 dwarfs and the K giants separately. We used a maximum likelihood algorithm for obtaining the space densities. We arrived at the following main conclusions in our paper: The absorbing material concentrates closer than 150 pc in our area. There is a weak but still significant correlation between the optical measures of absorption and the IRAS 100 micron Sky Flux Maps data. The spatial densities of F8 - G5 dwarfs essentially reflect the densities obtained in the galactic plane. The distribution of distance moduli of K giants in our sample can be well modelled by the z = r sin(b) scaling of Upgren's data from the North Polar region. The actual form of the space density curve of the K giants can be satisfactorily fitted both by an isothermal model and an exponential model.

Key words: late-type stars - galactic structure - multicolour photometry - interstellar matter

1. INTRODUCTION

The disk of our Galaxy is strongly flattened and therefore the stellar distributions obtained in any line of sight are essentially the projections of the vertical distribution into the particular direction observed, even at great angular distances from the galactic caps. In our previous papers (*Balázs* 1975, 1977, 1984, *Paparó and Balázs* 1982, *Balázs* et al. 1985) we focussed our attention mainly on the *A* type stars at low galactic latitudes of about +15 degrees. With this choice one can check whether the spatial distributions observed in the galactic polar caps are still held after suitable scale trans-

formation at greater angular distances from the polar direction or, on the contrary, one can pick up the possible deviations from a strict plane-parallel case. We have concluded that the spatial distributions obtained in the particular low latitude directions we studied can be satisfactorily described by the density laws in the polar cap directions after suitable scaling, i.e. substituting of $z = r\sin(b)$ into $D(z)$, where $z, r, b, D(z)$ mean the distance from the galactic plane, the distance in the line of sight, the galactic latitude of the field observed, and the density distribution of the stars in the polar caps, respectively. In two fields (a field in the Lyra and one around IC 4665) we found a good fit with the observed data by the suitably scaled model of *Woolley and Stewart* (1967), whereas the best fit was obtained by the isothermal model of *Bahcall* (1984) in the field around NGC 7686.

Unlike the *A* type stars at low galactic latitudes the physical background behind the observable distribution of *F* and later type stars is more complicated because in this case the lifetime of the objects is comparable with those of the Galaxy, and consequently we see a superposition of objects representing quite different stages of the dynamic and chemical evolution of our stellar system. A higher number of significant physical quantities is therefore required to describe the photometric and spectral properties of stars in the sample. In the case of main sequence *A* type stars the effective temperature and the interstellar reddening satisfactorily characterize the optical photometric properties of these stars. With the late-type stars, however, one has to add a further quantity describing the possible differences in chemical composition among the stars in the sample.

In statistical studies the most widely used photometric systems are the *UBV* and *RGU* systems because one can easily implement them on panoramic detectors (like CCD-s or photographic plates) and they are therefore well suited to statistical studies. In this paper we try to join the power of the *UBV* and *RGU* systems supplemented with small scale spectral classification in order to get a more reliable estimation of the physical parameters of stars in our sample. Our main purpose in this paper is the study of the vertical cross section of our Galaxy as free from a priori assumptions as possible.

2. OBSERVATIONAL MATERIAL AND DATA REDUCTION

Our work is based on the observations we made with the 60/90/180 cm Schmidt type telescope of the *Konkoly Observatory*. The spectra were obtained on IIa-O plates using a 5 degree ultraviolet transparent objective prism with a dispersion of 580 Å/*mm* at $H\gamma$. We widened them by 18" corresponding to 0.16 mm on the plate. The spectral and *UBV* plates were the same as those used when studying the *F7* and earlier type stars around IC 4665 (*Paparó and Balázs* 1982).

2.1 Multicolour photometry

As we mentioned in the introduction we have attempted to join the power of UBV and RGU photometry to get a more reliable estimation of the basic physical quantities of the stars in the sample. As a consequence we have supplemented our previous observational material with the R and G colours. The emulsion types, filters and exposures used are summarized in Table 1.

Table 1.

	Emulsion	Filter	Exp. time
U	Kodak 103a-O	Schott UG1 2mm	10 min
B	Kodak 103a-O	Schott GG13 2mm	5 min
V	Kodak 103a-D	Schott GG14 2mm	4 min
G	Kodak 103a-O	Schott GG5 2mm	10 min
R	Kodak 098-02	Schott RG5 2mm	10 min
Spectral plates	Kodak IIa-O	5° prism	24 min

The limiting B magnitude of the survey was about 13.5 mag. It was defined as the faintest star in the sample, but the limit of completeness is about 1.5 mag brighter. Fig.1 shows the distribution according to the apparent B magnitude of all program stars, $F-G$ stars and K stars, separately. For the calibration of both photometric systems we used *Alcaino*'s (1965) UBV photoelectric measurements on IC 4665. The transformations between the instrumental and international systems are given by the following equations:

$$\begin{aligned} V_{instr} &= V - 0.145(B-V) + 0.079 \\ (B-V)_{instr} &= 1.040(B-V) - 0.055 \\ (U-B)_{instr} &= 1.040(U-B) - 0.007 \end{aligned}$$

The calibration of RGU colours proceeds utilizing UBV photoelectric standards. There are two implementations of this photometric system, i.e. the version of *Steinlin* (1968) and that of *Buser* (1978a,b). We tried both of them and got the impression that *Buser*'s was better suited to the data, and we therefore used this version in our work. The transformation of UBV standards into RGU requires knowledge of the $E(B-V)$ interstellar reddening of the standards. The published reddening measurements for this field (*Paparó and Balázs* 1982) revealed that the value varies between 0.2 and 0.3 mag. over the whole field in the case of distant stars. This means that except for the distant giant stars this term could be omitted from the transformation equations.

Table 2.

spectral type	criteria used for classification
F8	G-band $\leq H\gamma$ CaI4227 appears in luminosity class *V*. FeI4325 is noticeable.
G0	G-band $\approx H\gamma$ and CaI4227 $\approx H\delta$ FeI4325 $< H\gamma$
G2	G-band $> H\gamma$ and FeI4325 $< H\gamma$
G5	G-band $\gg H\gamma$ and FeI4325 $\geq H\gamma$
G8	G-band $\gg$ CaI4227 and FeI4325 $> H\gamma$
K0	CaII(H) and (K) at maximum strength H-lines disappear CaI4227 < G-band
K2	Continuum becomes weak in blue. CaI4227 < G-band Metallic blends appear.
K5	The strength of G-band is equal to CaI4227. Strong metallic blends in all spectral regions. (G-band is stronger than CaI4227 in all *K* types of highest luminosity classes.)
M0	TiO bands noticeable and CaI4227 $\gg$ G-band. The spectral pattern is dominated by λ4227 in luminosity class *V*. λ4227 decreases with increasing luminosity class.
M5	Spectrum fluted by strong molecular bands.

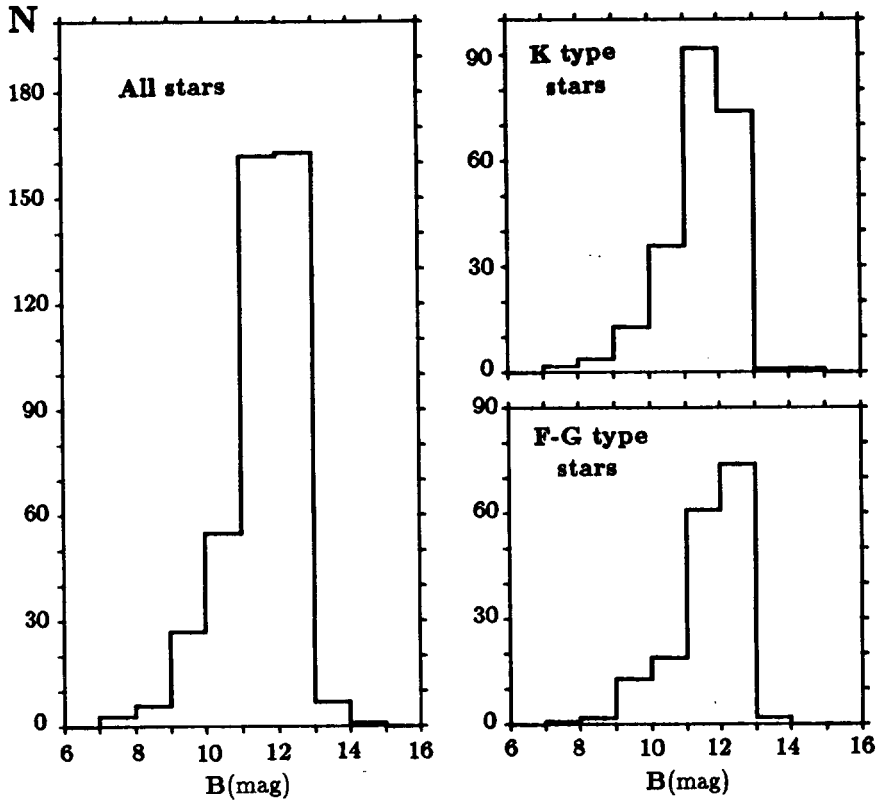

Fig. 1a-c. Distribution of stars according to the B magnitude (all stars, F - G type and K type stars respectively). The sharp edges at the right side of the diagrams are due to the magnitude limit of our sample.

Based on these calibrations we determined the photometric colours of the program stars using the Cuffey type iris photometer of the *Konkoly Observatory*. We measured 5 plates in UBV and 3 plates in the R and G colours. The corresponding accuracy of photometric magnitudes obtained in this way are ± 0.07, ± 0.06, ± 0.05, ± 0.08 and ± 0.06 magnitudes for U, B, V, R and G respectively. The photometric data of our program stars in the international system are summarized in Table 6.

2.2 Spectral classification

The spectra obtained by the 5 degree prism were classified visually using the criteria of the Bonner Spectral Atlas (*Seitter* 1975). According to the sharpness of the criteria we can define the following normal groups (a concept introduced in *Morgan* 1951) to assign those stars which are indistinguishable from each other in respect of the given criteria and dispersion of spectra. Considering the resolving power of our

5 degree prism and the widening of our spectra we can set up the following groups: *F8, G0, G2, G5, G8, K0, K2, K5, M0, M5.*

We used the following general features in our work: Balmer lines decrease with advancing spectral type and disappear around *K0.* The spectral pattern is dominated by the CaII(H) and (K) lines, G-band and strong absorption in the region $\lambda 4118-4216$ in the blue part of the spectrum. The CaI4227 increases rapidly with advancing spectral type after the *K0.* Blend MnI, FeI, SrII $\lambda 4031-4078$ becomes increasingly strong with advancing spectral type and is the dominating feature in the blue spectral region of stars later than *G5* and luminosity classes *V.* TiO bands appear around *M0* and increase towards later types. $\lambda 4215-4227$ is intense and $\lambda 4200, 4176, 4155$ bands are noticeable in spectral type *K* at luminosity class *III.* The characteristic features of spectral groups are listed in Table 2. We have based our further discussion on these subgroups supplemented with multicolour data.

3. INTERSTELLAR REDDENING

Before entering into the details of the space distribution of stars of different spectral characteristics based on photometric parallax, we have to remove the effect of interstellar reddening from the photometric data. Spectral classification of small scale spectra enables us in principle to estimate the intrinsic colours of the stars and compare them with those actually measured. In the case of stars of *F8* and later, however, one encounters difficulties. The reddening path of late-type stars on the $B-V$, $U-B$ and $G-R$, $U-G$ two-colour diagrams makes a much smaller angle to the unreddened branch of Population I stars in these diagrams, unlike stars of *A5-F5* spectral types (see the model calculations of *Buser* 1978a). As a consequence, even small errors in the spectral classification could cause serious bias in determining the colour excesses in this way. An additional difficulty arises from the photometric effect of differences in chemical abundances. The blanketing effect, i.e. the photometric differences of stars due to their metal abundances, can become quite prominent among spectral types of *F5* and later, especially at higher galactic latitudes. The blanketing shifts the stars to the right and upwards on the two-colour diagrams. Both the reddening and the blanketing shift the stars rightwards on the two-colour diagrams but in the $U-B$ or $U-G$ direction, on the contrary, the results of these two effects are just the opposite: the reddening shifts downwards while the blanketing shifts upwards. If one knows the spectral type, therefore, one can in principle distinguish between these two effects. In reality, however, due to the uncertainty of spectral types of *G-K* stars on our small scale spectra, one encounters difficulties when trying to separate the blanketing from the reddening in this way. To study the distribution of absorbing material responsible for the interstellar reddening in this field, we therefore have to invoke the results of other investigations as well. The overall galactic optical absorption due to interstellar

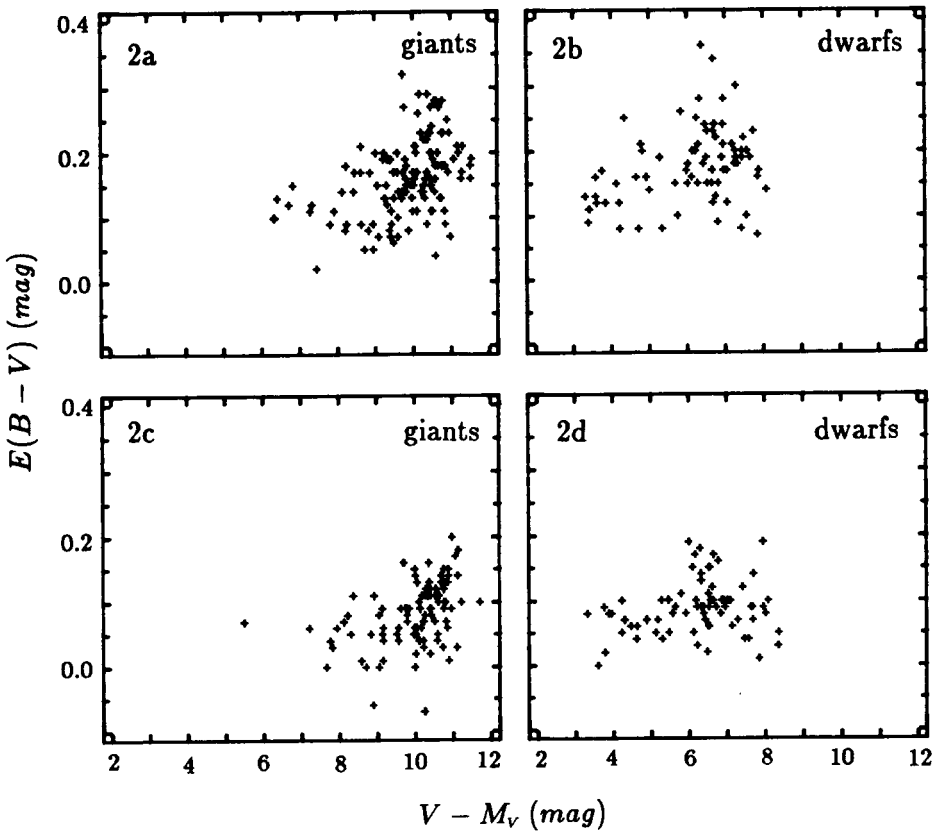

Fig. 2.a-d Plot of the E(B-V) colour excesses of the program stars, estimated by factor analysis, versus uncorrected distance moduli. (a-b: below and c-d: above the 425th line in the PL113 IRAS Sky Flux map). Note the similarity between the distribution of colour excesses of giants and dwarfs indicating the presence of a nearby obscuring cloud.

dust was studied by *FitzGerald* (1968) and *Neckel and Klare* (1980). The spatial resolution of their studies was fairly poor owing to the sparseness of stars in our 19.5 sq. degree field. Nevertheless, their studies indicated that the surface density of the absorbing material was non-uniform, i.e it was mostly concentrated in the smaller galactic latitude side of our field; and both studies showed an abrupt increase in the absorption within 200 pc, revealing the presence of a nearby absorbing cloud. These results were confirmed by our previous study on the distribution of stars of types *F7* and earlier based on 427 stars (*Paparó and Balázs* 1982). To get a more detailed picture of the distribution of absorbing material in our field we invoked the relevant IRAS Sky Flux Map. To compare the IRAS colours with our photometric data we sampled the 100 μm map of the PL113 plate at the positions of our program

stars. Since the 100 μm radiation originates predominantly from the galactic dust clouds (*Hauser et al.* 1984) and the IRAS fluxes represent the total column density of the emitting material, we may expect good correlation with the optical absorption only with stars which are lying behind the absorbing material in the line of sight. The dust particles emitting the IRAS fluxes and those responsible for the optical absorption are not necessarily identical. Furthermore, the dust clouds may differ in their characteristic temperatures causing different infrared properties without affecting the optical properties of the absorbing material. All these effects work against a close correlation between the optical absorption and the measurable FIR radiation of the dust clouds. Our expectation is therefore only justified when the distribution of dust particles responsible for the infrared radiation is similar to the distribution of those making the optical absorption and there are no big differences in the temperatures of dust clouds in our area. A further difficulty arose from the influence of the Zodiacal Light dominating the 12 μm and 25 μm radiation in our field. It was an unfortunate circumstance that the general trend of the Zodiacal emission nearly corresponded to those of the interstellar reddening in our case. We cannot exclude the possibility that the correlation between the optical obscuration and the FIR might originates from this coincidence. Nevertheless, a comparison between the optical measures of absorption and the intensity of the FIR radiation may also have some significance.

To obtain a reliable measure for the optical absorption we tried to concentrate in one variable all the information our photometric data contained in respect of interstellar absorption. As we mentioned earlier in this paper the interstellar reddening shifts the stars rightwards to the unreddened loci of objects on the $B-V$, $U-B$ and $G-R$, $U-G$ two-colour diagrams. The orthogonal distance from the unreddened two-colour line due to this shift, depends on the spectral type and the actual functional form of the line joining the unreddened loci of objects in these diagrams. In the case of Population I objects this functional form is well approximated by straight lines in the following spectral ranges, based on the calibration of *Buser* (1978a):

- in the *F8-K0* spectral range the loci of dwarfs and *G5-G8* giants essentially define the same straight line on the two-colour diagrams within the accuracy of our photometric data;

- in the *K0-M0* domain, in contrast, the giants and dwarfs populate different lines;

- in the *M1* and *M6* domain the giants are well approximated by a straight line but both the photometric measurements and calibrations are rather uncertain because of the increasing dominance of molecular bands in this range. We assigned to all of these stars the spectral type *M5* in our sample. Because of the great uncertainties in their photometric data we omitted them from the further analysis.

Assuming that the real functional form can be well represented by these straight lines and, furthermore letting $B-V$, $U-B$, $G-R$ and $U-G$ be the respective measured colour indices in the UBV and RGU systems, then the orthogonal displacements of stars from the unreddened Population I two-colour lines can be written in the form of the equations:

$$DUBV = \alpha_1(B-V) + \beta_1(U-B) + \gamma_1$$
$$DRGU = \alpha_2(G-R) + \beta_2(U-G) + \gamma_2$$

The following table summarizes the value of coefficients in these equations, in the spectral ranges mentioned above.

Table 3.

	α_1	β_1	γ_1	α_2	β_2	γ_2
F8-K0 dwarf	+0.839	-0.543	-0.444	+0.815	-0.578	-0.006
K2-M0 dwarf	+0.761	-0.648	-0.202	+0.773	-0.634	+0.304
K0-M0 giant	+0.875	-0.481	-0.418	+0.869	-0.495	-0.039

These displacements may not only be due to interstellar reddening but may be partly accounted for by the blanketing effect. To get more information on these two physical quantities and to study their influence on the measured colours separately and in more detail, we subtracted the respective colour indices estimated on the basis of the spectral types of our program stars from the actually measured colour indices, i.e.:

$$EUB = (U-B) - (U-B)_0 \quad , \quad EUG = (U-G) - (U-G)_0$$
$$EBV = (B-V) - (B-V)_0 \quad , \quad EGR = (G-R) - (G-R)_0$$

The '$_0$' indices denote *Buser*'s normalized synthetic colours corresponding to the unreddened Population I values of the spectral types of our program stars. Although all of these quantities have some relevance in measuring the amount of optical absorption, we omitted from our further study the short wavelength colour differences, i.e. EUB and EUG, because blanketing affects them much more seriously; as it does the possible uncertainties that may be present in the spectral classification.

To concentrate the photometric effect of interstellar absorption into one variable we proceeded to estimate its effect contained in EBV, EGR, $DUBV$ and $DRGU$. To

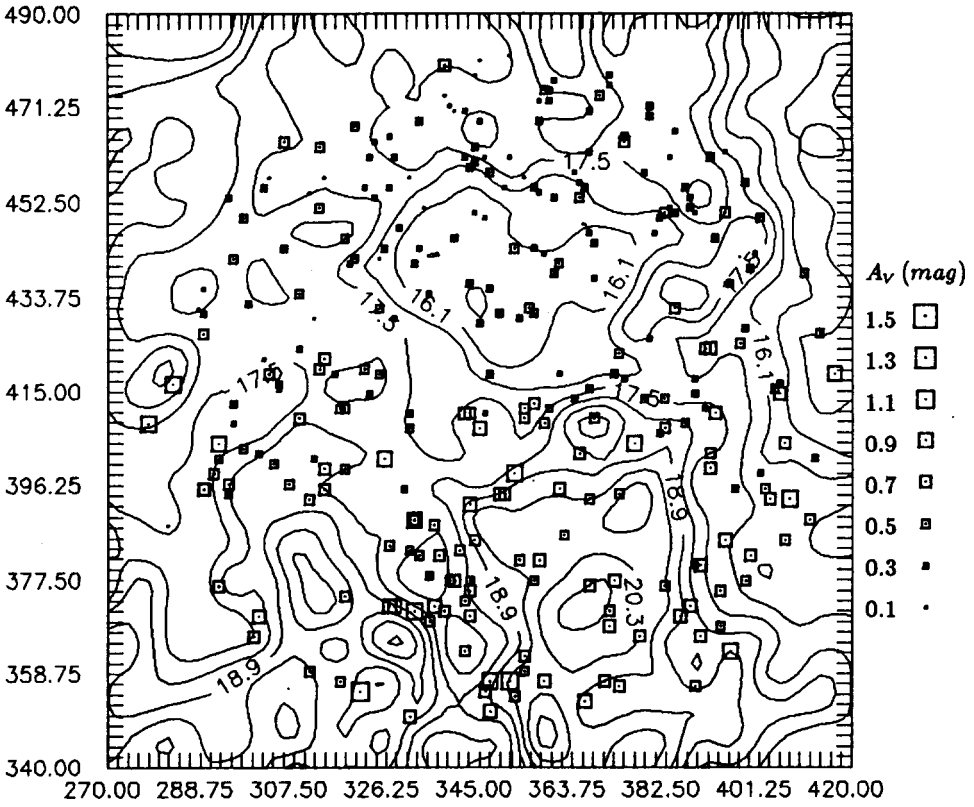

Fig. 3. Comparison of the 100 micron IRAS flux with the estimated visual absorption. Sizes of squares are proportional to the measure of visual absorption at the place of program stars. Both the 100 micron flux and the optical absorption are stronger in the southern part of our field. The numbers at the left side and the bottom of the figure refer to the lines and columns in the PL113 IRAS Sky Flux Map.

carry out this procedure we invoked a standard technique of multivariate mathematical statistics, factor analysis. According to the basic assumption of factor analysis we suppose that the components of an $\mathbf{X}$ observable m-dimensional statistical variable can be well represented by the linear combination of k other variables, called factors. This means

$$X_j = \sum_{l=1}^{k} c_{jl} f_l + e_j \quad , \qquad j = 1, ...m \text{ and } k < m$$

where c, f and e are the factor coefficients (loadings), factor values (scores) and individual factors, respectively. There are a wide variety of methods published in the

literature for estimating the different components of factor models . We used the solution based on principal components analysis (for further details on this method see *Murtagh and Heck* 1987). The factors obtained by principal components analysis are always uncorrelated. We have identified the components of $\mathbf{X}$ with EBV, EGR, $DUBV$ and $DRGU$ and therefore $m = 4$ in our case.

Performing factor analysis on our data field we got a set of uncorrelated variables describing the basic dependences between the variables observed. We made the assumption that there were some physical variables (interstellar reddening and blanketing in our particular case) behind the observed ones and that they determined the variables actually observed. If the transformation between this physical variables and those observed were linear we might expect some linear connection between the physical and factor variables as well.

The number of significant factor variables set an upper limit for the number of physical variables one can recognize in the given data field. To ensure the validity of the required linearity we performed the factor analysis in the spectral groups defined above, separately. According to the principal components analysis technique the variables measured were represented by linear combinations of eigen vectors of the correlation matrix of the variables observed. Factor analysis then proceeded by dropping eigenvectors with small eigenvalues and assumed only those to be significant which were above a certain threshold. In the SPSS software package what we used in computing the factor model, the default value of this threshold was set to equal 1. Table 4. summarizes the eigenvectors of the correlation matrix in the case of the *F-G* dwarfs and the *K* giants separately:

Table 4.

	F-G dwarfs		K giants	
factor	eigenvalue	cum.pct.	eigenvalue	cum.pct.
1	2.898	72.4	2.566	64.2
2	.860	93.9	.810	84.4
3	.213	99.3	.592	99.2
4	.029	100.0	.032	100.0

Examining Table 4. one can infer that in both cases there is only one eigenvalue lying above the default threshold. The second eigenvalues, however, are close to unity and we tried to reproduce the covariance matrix keeping these factor variables. In the case of the dwarf stars the use of these two factors gave satisfactory reproduction of the covariance matrix. In the case of giants this reproduction was not so good but was still acceptable. We therefore used these two factors in our further calculations.

There are no clear rules concerning the making of comparisons between the variables obtained by factor analysis and those representing real physical quantities. Since the 100 μm IRAS fluxes are good measures of the amount of galactic dust, we identified those factor variables with interstellar absorption which showed the maximum correlation between the intensity of FIR radiation and the factor values given by the analysis. We expected correlation between the optical measure of absorption and the 100 μm flux only with those stars which are lying at greater distances than the bulk of emitting dust material responsible for the FIR radiation and detected by the IRAS mission.

3.2 Distribution of the absorbing material

We plotted the estimated colour excesses against the distance modulus of the stars in our sample in Fig. 2a-d for giants and dwarfs separately. We divided the whole field by the 425. line of the respective IRAS Sky Flux map in order to demonstrate the assimmetry in the surface distribution of the obscuring material over the whole area. It was also apparent on these plots that there were no significant difference between the distributions of the optical absorption of dwarfs and giants. Furthermore, the absorption of dwarfs increased up to 0.7 mag near to 6.7 of uncorrected distance modulus and did not change remarkably among the giants. It means that the vast majority of the absorbing material was concentrated within the distance modulus near

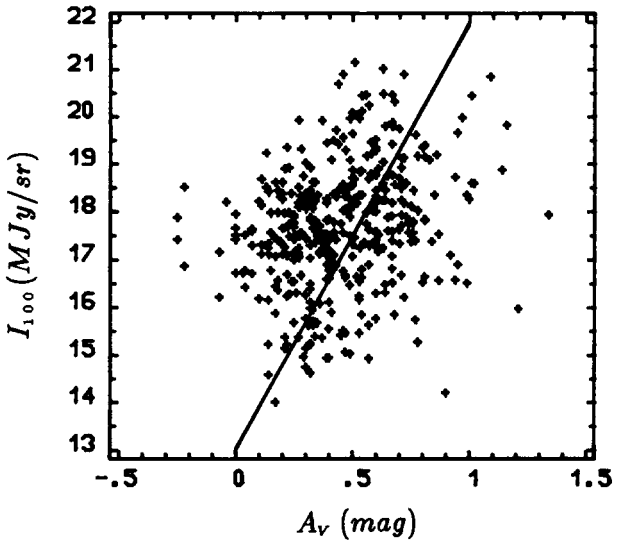

Fig. 4. Correlation between 100 micron IRAS flux and the estimated visual absorption. A line with 9 MJy/Sr per magnitude slope, found by de Vries and Le Poole (1985) for some high latitude dust clouds is also indicated.

to 6 corresponding to a distance of about 150 pc. We might therefore expect correlation between the IRAS fluxes and the stellar reddening with those stars which were lying behind this distance. The surface distribution of absorbing material was not uniform in this area, as was suggested by the earlier investigations. The patchy structure of the interstellar dust is also apparent on the IRAS Sky Flux maps. We plotted the reddening data of stars of $r > 150$ pc, represented in Fig. 3, in order to make a comparison between the surface distribution of the optical absorbing material and the FIR radiation. By doing this we recovered the results of the earlier investigations but with better angular resolution.

To get reliable correlation between the optical and infrared data we divided the stars in our sample into three groups: dwarfs $r < 150$ *pc* $(V - M_V < 6.7)$, dwarfs $r > 150$ *pc* and giants. Table 5. shows the correlations between the factor values and the 100 μm flux within each of these groups:

Table 5.

	dwarfs1			dwarfs2			giants		
	Flux.	$f1$	$f2$	Flux.	$f1$	$f2$	Flux.	$f1$	$f2$
Flux.(100)	1.00	.06	-.07	1.00	.33*	.18	1.00	.25**	-.03
$f1$	.06	1.00	.07	.33*	1.00	.01	.25**	1.00	.00
$f2$	-.07	.07	1.00	.18	.01	1.00	-.03	.00	1.00
number of cases:		91			52			204	

1-tailed Signif: * - 0.01 ** - 0.001

Examining this table one can clearly see that factor $f1$ has significant correlation with the FIR radiation in two of the groups, whereas $f2$ has not. The lack of significance in the first group and the significance in the second and third ones reflect the fact that the optical absorption, and also the FIR radiation, originate from a nearby dust cloud. Fig. 4 summarizes the dependence of the optical absorption measures on the 100 μm radiation. We computed a best fitting line to the points in this figure by extracting the common factor in A_V and 100 μm flux. The shape of this line was 5.4 MJy/Sr/mag while *de Vries* and *Le Poole* (1985) obtained 9 MJy/Sr/mag for some high latitude extended dust clouds. We adopted the estimated value of $f1$ as a measure of the optical absorption and converted it into factor-analysis-predicted EBV and EGR using the linear relation between the colour excesses and the factor values. The measure of the optical absorption can be obtained using the standard relationship between selective and total absorption. We used here the coefficients published by *Buser* (1978a).

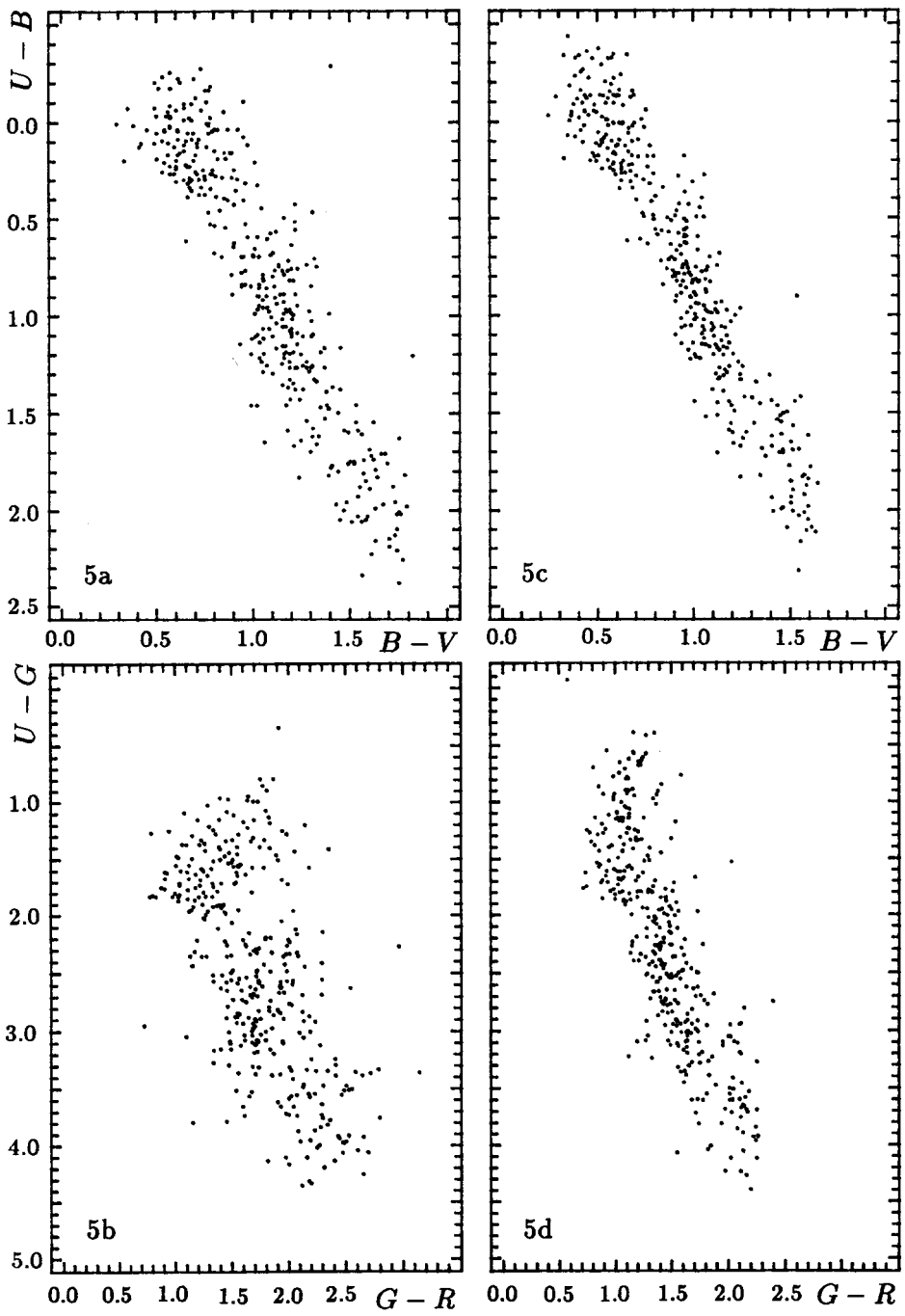

Fig. 5. Two-colour diagrams in UBV and RGU systems. Without (5a-b) and after (5c-d) correcting for the estimated interstellar reddening.

4. SPATIAL DISTRIBUTION OF THE STARS

4.1 Generalization of the convolution equation for multivariate case

After eliminating the effect of the interstellar reddening we could proceed to the determination of the spatial distribution of our stars. To check the reliability of the procedure we used for the elimination of reddening from our data we compared the two-colour diagrams of the non-corrected colour indices with those corrected using the method described in the previous paragraph. The power of this procedure is demonstrated in Fig. 5. To derive the space densities of our stars we made the usual assumption that their true absolute magnitudes are represented by a Gaussian random variable with a mean value given by their spectral type, luminosity class, chemical composition and σ standard deviation (*McCuskey* 1966). We have a multicolour sample in our case and consequently the absolute magnitude itself is also a multivariate Gaussian random variable with a mean according to the spectral characteristics of the stars and a Σ covariance matrix. We have omitted from the further calculations the U colour because, as we pointed out in the previous paragraph, the errors inherent in spectral classification affect this spectral band most seriously. Let

$$\Phi(\mathbf{M}|Sp) = \frac{exp(-(\mathbf{M}-\mathbf{M0})^T \Sigma^{-1}(\mathbf{M}-\mathbf{M0}))}{(2\pi)^{m/2} DET(\Sigma)}$$

a multivariate Gaussian where $\mathbf{M}$ represents the set of variables B, V, R and G (so we have a four dimensional variable in our case), Sp the spectral type given, $\mathbf{M0}$ the mean value of absolute magnitude and Σ the covariance matrix. With these notations we can generalize the standard integral equation of stellar statistics (*Kurth* 1967) in the form of

$$A(\mathbf{m}|Sp) = \int_{-\infty}^{+\infty} \Delta(\rho)\Phi(\mathbf{m}-\rho \mid Sp)d\rho$$

Where $\mathbf{m}$ and ρ are multivariate random variables representing the apparent magnitudes and distance modulus in different colour bands while A and Δ stand for their probability densities respectively. To solve this integral equation we approximated the integral expression with a sum of

$$A(\mathbf{m}|Sp) = \sum_{l=1}^{k} q_l \Phi(\mathbf{m}-\rho_l \mid Sp) \qquad l = 1, ..., k$$

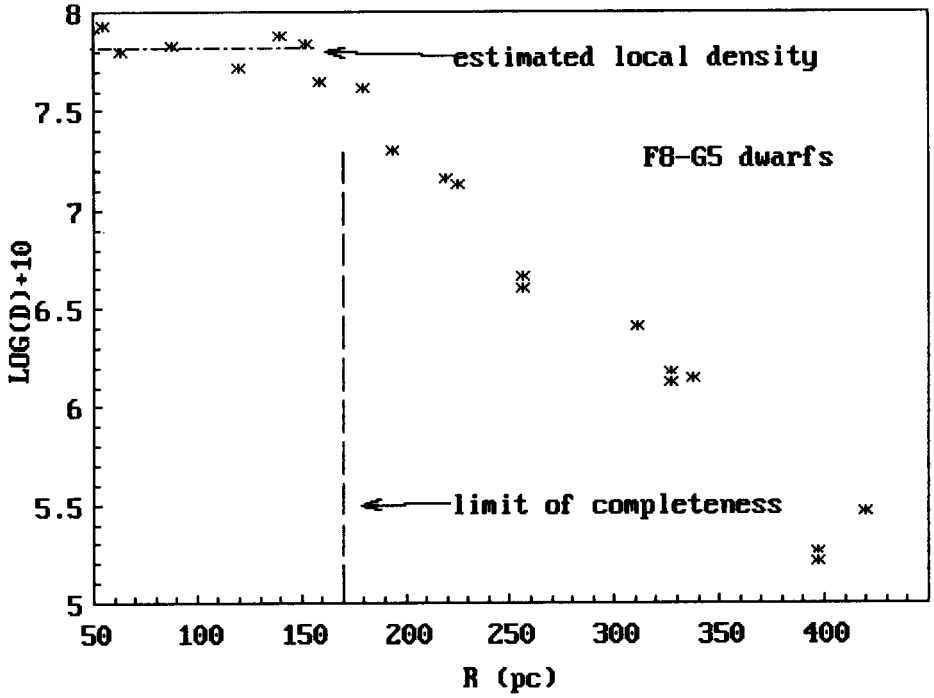

Fig. 6a. Dependence of logarithmic density on the distance in line of sight in case of F8-G5 dwarfs. The limit of completeness of our sample is marked by a vertical dashed line.

containing $q_i = \Delta(\rho_i)d\rho$ and ρ_i as unknown parameters to be determined. To estimate the set of the unknown parameters we used the maximum likelihood method. We defined the maximum likelihood function in the usual way:

$$L(\mathbf{a}) = \sum_{i=1}^{n} log A(\mathbf{m}_i \mid Sp).$$

In this equation **a** represents the set of parameters to be estimated and n the size of the sample. The maximum likelihood principle requires the estimation of those values of **a** which maximize $L(\mathbf{a})$, i.e.:

$$\frac{\partial L(\mathbf{a})}{\partial \mathbf{a}} = 0.$$

The derivatives of L(**a**) yielded a system of equations and the solution of this system resulted in the parameter values we were looking for. In the following we discuss the

results of these computations in separate spectral subgroups.

4.2 F8-G5 stars

The $F8 - G8$ stars formed a separate group in our two-colour diagrams. After being corrected for interstellar reddening they satisfactorily concentrated along the unreddened main sequence line in the two-colour diagrams. We cannot distinguish among the subdwarfs, dwarfs, subgiants and giants in this spectral region using our small scale spectra. Using larger dispersion spectra for a magnitude limited sample, *Kharadze* et al. (1989) concluded that among their G type stars there were practically the same numbers of subgiants and dwarfs. On the other hand, in *Houk*'s (1983) HR diagram based on the Michigan spectral survey data, the stars mainly populated the main sequence in the $F8 - G5$ region. *Kharadze* et al. assigned all stars to subgiants which could not be classified as either giant or dwarf. Their number of subgiants may therefore perhaps have been overestimated. We made the assumption in our further analysis that the vast majority of our $F8 - G5$ stars belonged to the main sequence dwarfs.

As a result of the reddening correction a small number of the stars were shifted above the main sequence line. Their corrected position corresponded to those produced by the blanketing effect. The shift gave an ultraviolet excess of about 0.2 mag in the UBV and 0.3 mag in the RGU system and might be explained by metal deficiency in these stars. Measurements using a more sophisticated photometric system such as the Strömgren *uvby* photometry could prove the validity of this conclusion. With the exception of these UV objects we assumed that the $F - G$ stars were main sequence stars in our sample and assigned to them absolute magnitudes according to their spectral types given by *Allen* (1973).

The absolute magnitude increases very rapidly within this spectral group. From the value of 4.0 at $F8$ stars it reaches 5.5 at $G8$ in the V band. Since our sample was magnitude limited the limiting distance in our sample, i.e. the distance which the space densities were biased beyond, varied strongly from $F8$ to $G8$ as well. To get a greater limiting distance but still enough objects to make statistical studies we restricted ourselves to the spectral range of $F8 - G5$.

Performing the maximum likelihood algorithm outlined above we obtained an estimation of the space densities as a function of the distances from the Sun. Fig. 6a shows the logarithm of these densities as a function of the distances. The limit of completeness is also indicated. The points obtained run nearly horizontally in the unbiased range of the diagram. Since the limiting distance is about 250 pc in our case, the distance from the galactic plane is less than 70 pc in the unbiased range. This means that we are practically seeing the space density of $F8 - G5$ stars in the galactic plane.

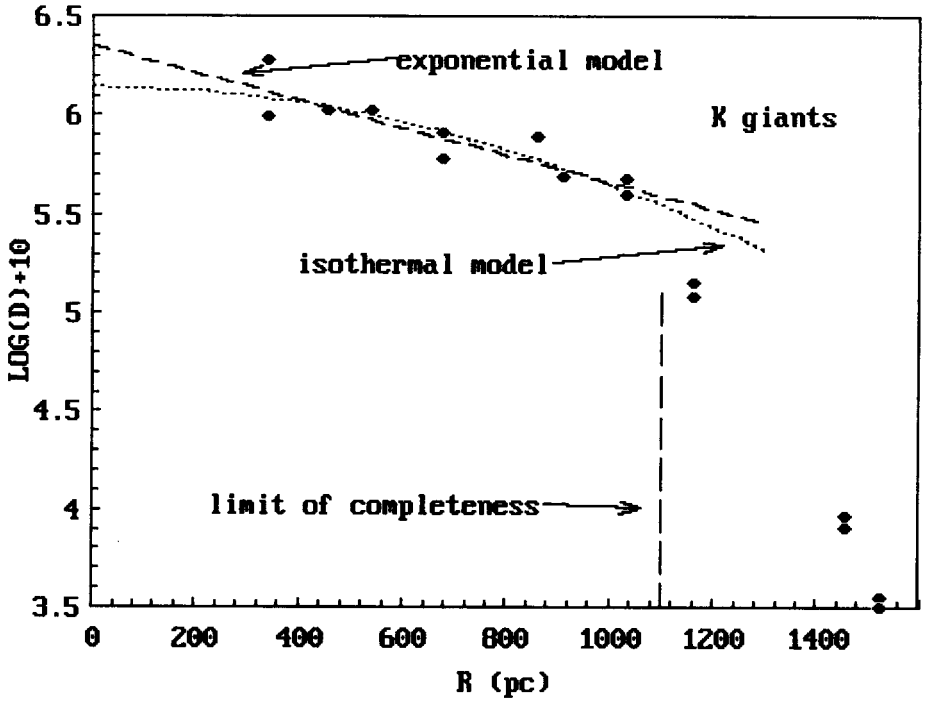

Fig. 6b. Dependence of logarithmic density on the distance in line of sight in case of K giants. The limit of completeness of our sample is marked by a vertical dashed line. Our fits with an isothermal and an exponentional model are also indicated.

4.3 K giants

The separation of K giants from the dwarfs is in principle possible on our small scale spectra. In practice, however, we succeeded in doing it with satisfactory reliability only with stars having well exposed spectra on our plates, i.e. with the brighter stars in our sample. Most of these stars appeared to be giants which nicely followed the line of the Population I giants on the two-colour diagrams after being corrected for reddening. The majority of fainter stars not bright enough for reliable luminosity class estimation also concentrated along the Population I giant line. In some cases, however, we had stars departing significantly from this line. In a considerable number of these cases the photometric images of objects in one of the colours distorted by a neighbouring star or the U colour was too faint for reliable brightness determination. Of course, we could not exclude the possibility that some of them were dwarfs, especially those lying along the dwarf line, or metal poor giants, if their positions on the two-colour diagram were realistic. Again, more accurate photometric or spectroscopic measurements would be

desirable in these cases. We also omitted from the further analysis the stars with spectral types later than $M0$. We rejected 35 stars altogether in this way. Assuming that the stars remaining in the sample were Population I giants we assigned absolute magnitudes to them as given by *Allen* (1973). The space densities yielded by the maximum likelihood algorithm are displayed in Fig. 6b.

The main aim of our studying the space densities in this low latitude field was to compare spatial distributions in the galactic caps with those obtained in the present investigation. In particular, we were interested in testing the plane-parallel hypothesis, i.e. the hypothesis that the low latitude distributions can be well approximated by the substitution of $z = r\sin(b)$ into $D(z)$, the density in the direction of the polar caps, due to the high flattening of the galactic disc. The most extensive study in the direction of the North Polar Cap was the work of *Upgren* (1962) containing 4027 stars of spectral class $G5$ and later in a 396 square degree field down to a limiting photographic magnitude of 13.0 . We tested this hypothesis by substituting $z = r\sin(b)$ ($b = +16°.5$ in our case) into *Upgren*'s density data and converted them into the distribution of the distance moduli which was the output of our maximum likelihood algorithm. The result of this comparison is shown in Fig. 7. This figure demonstrated with satisfactory significance that our points followed *Upgren*'s transformed curve up to a distance modulus of 10 mag corresponding to the limit of completeness in our sample . It has also been demonstrated that the plane-parallel approximation holds at least up to 1000 pc from the Sun in this direction.

In Fig. 6b we have shown the logarithmic space density of K giants of our sample as a function of the distance in the line of sight. The usual assumption that the space density is well approximated by an exponential function with a scale height depending on the absolute magnitude (see e.g. *Bahcall and Soneira* 1980) would result in a straight line in this figure. The scale height of the best fitting line corresponded to 200 pc perpendicular to the galactic plane. Assuming an isothermal model, on the other hand, we get

$$logD(z) - logD(0) = -\frac{u(z)}{\sigma_W^2}$$

where the gravitational potential $u(z)$ is well approximated by

$$u(z) \approx u(0) - \frac{u(0)''}{2}z^2$$

near to the galactic plane. This analytical form of the logarithmic density also fits satisfactorily with our data.

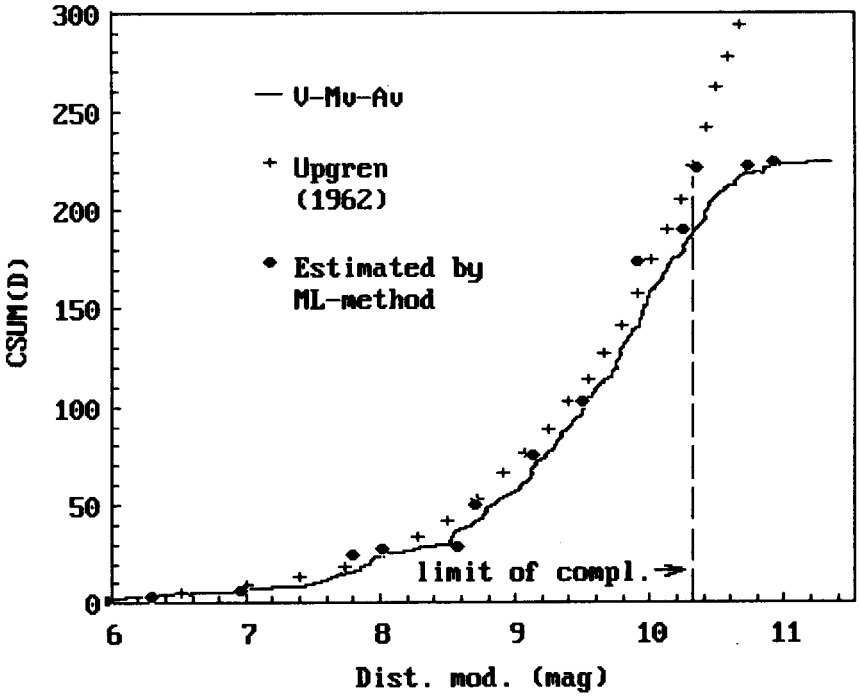

Fig. 7. The cumulative space density of K-type stars plotted against distance moduli for our program stars (full line) and for Upgren's (1962) data (crosses) after $z = r\sin(b)$ scaling. Departure from Upgren's data above 10 magnitude is due to the incompleteness of our sample in that range.

5. CONCLUSIONS

We have investigated 424 stars of spectral types of $F8$ and later in a 19.5 sq. degree field around IC 4665. The main purpose of our study was to make comparisons between the space densities of late-type stars in the galactic caps with samples taken from fields at great angular distances from the poles ($b = +16°.5$ in our case). In particular, we were interested in testing the plane-parallel hypothesis of the density distribution, i.e. the hypothesis that the spatial density of the Population I stars observed at great angular distances from the galactic caps is well approximated by the $z = r\sin(b)$ scaling of the distributions obtained in the polar regions.

The major difficulty in making the comparison between our field and the polar region is the adequate treatment of the patchy distribution of the interstellar obscuring material over the field investigated and its elimination from the photometric data. To

get an adequate estimation of the effect of the absorption we joined the power of the UBV and RGU photometric systems combined with the results of classification on small scale spectra. These data enabled us to get $E(B-V)$, $E(G-R)$ and perpendicular distances from the unreddened loci of the Population I stars in the two-colour diagrams, $DUBV$ and $DRGU$. We used the factor analysis of multivariate mathematical statistics in order to extract the effect of absorption from the data field defined by EBV, EGR, $DUBV$ and $DRGU$. To identify the factor component corresponding to the interstellar reddening we invoked the corresponding IRAS Sky Flux Data. After removing the interstellar reddening from our photometric data we computed the spatial densities for the $F8-G5$ dwarfs and the K giants separately. We used a maximum likelihood algorithm for obtaining the space densities from the photometric data. We can summarize the main conclusions of our paper as follows:

1. A significant amount of the absorbing material concentrates closer than 150 pc in our area producing $A_V = 1\ mag$ at the densest part of the obscuring cloud.

2. There is a weak but still significant correlation between the optical measures of absorption and the IRAS 100 μm Sky Flux Maps data. The shape of the best fitting line between A_V and 100 μm flux equalled 5.4 MJy/Sr/mag.

3. The spatial densities of $F8-G5$ dwarfs essentially reflect the densities obtained in the galactic plane. In a few cases UV excess seems to be present but this needs further confirmation based on measurements in more sophisticated photometric systems.

4. The distribution of distance moduli of K giants in our sample can be well modelled by the $z = r\sin(b)$ scaling of *Upgren*'s data from the North Polar region. The actual form of the space density curve of the K giants can be fitted by an exponential distribution with a scale height of 200 pc perpendicular to the galactic plane. A satisfactory fit can also be obtained by an isothermal model which is more realistic from the physical point of view. While the exponential model predicts a discontinuity in the density gradient at z=0, the isothermal version moves through this point with continuous derivative.

ACKNOWLEDGEMENTS

We are indebted to *Dr. M. Kun* for her useful advice in recognizing the *K* giants on our small scale spectra. We wish to thank *Dr. K. Ishida* (University of Tokyo) and *Dr. L. Szabados* for reading the manuscript and making valuable comments. We are also grateful to *Mr. Holl* for his kind help in picture processing the IRAS Sky Flux Maps and to *Dr. J. Kelemen* for his contribution in making the identification map. The kind permission for the relevant IRAS data by the *Huyghens Laboratory*, in particular the help of *Prof. H.J. Habing* and *Dr. E. Deul*, is also acknowledged.

Budapest - Szabadsághegy, Dec 20, 1990.

REFERENCES

Alcaino, G., 1965, *Bull. Lowell Obs.*, **6**, No.7, 167.

Allen, C. W., 1973, *Astrophysical Quantities* 3rd.ed., Athlona Press, London.

Bahcall, J. N., 1984, *Astrophys. J.*, **276**, 169.

Bahcall, J. N., Soneira, R. M., 1980, *Astrophys. J., Suppl. Ser.*, **44**, 73.

Balázs, L. G., 1975, *Mitt. Sternwarte Ung. Ak. Wiss.* **68**.

Balázs, L. G., 1977, The Cosmogonical Significance of the *z* Distribution of Stars in *"Chemical and Dynamical Evolution of our Galaxy"* IAU Coll. **45**, 271.

Balázs, L. G., 1984, Statistics of A-type Stars as Possible Indicator of Star Formation in *"Astronomy with Schmidt-Type Telescopes"* ed. Capaccioli M., D. Reidel Publ.Co. p.269.

Balázs, L. G., Paparó, M., Tóth, I., 1985, *Mitt. Sternwarte Ung. Ak. Wiss.* **85**.

Buser, R., 1978a, *Astron. Astrophys.*, **62**, 411.

Buser, R., 1978b, *Astron. Astrophys.*, **62**, 425.

de Vries, C. P., Le Poole, R. S., 1985, *Astron. Astrophys.*, **145**, L7.

FitzGerald, M. P., 1968, *Astron. J.*, **73**, 983.

Hauser, M. G., Gillett, F. C., Low, F. J., Gautier, T. N., Beichman, C. A., Neugebauer, G., Aumann, H. H., Band, B., Boggess, N., Emerson, J. P., Houck, J. R., Soifer, B. T., and Walker, R. G., 1984, *Astrophys. J.*, **278**, L15.

Houk, N., 1983, The Nearby Stars and the Stellar Luminosity Function, *IAU Coll. No. 67*, Ed. by Philip A. G. D. and Upgren A. R., L. Davis Press p.345.

Kharadze, E. K., Bartaya, R. A., Dluzhnevskaya, O. B., Piskunov, A. E., Pavlovskaya, E. D., 1989, *Astrophys. Space Sci.*, **151**, 319.

Kurth, R., 1967, *Introduction to Stellar Statistics*, Pergamon Press, Oxford.

McCuskey, S. W. 1966, *Vistas in Astronomy*, **7**, 141.

Morgan, W. W., 1951, *Publ. Univ. Michigan Obs.*, **10**, 33.

Murtagh, F., Heck, A., 1987, Multivariate Data Analysis, *Astrophys. Space Sci. Lib.*, **131**. D.Reidel Publ.Co.

Neckel, T., Klare, G., 1980, *Astron. Astrophys., Suppl. Ser.*, **42**, 251.

Paparó, M., Balázs, L. G., 1982, *Mitt. Sternwarte Ung. Ak. Wiss.* **82**.

Seitter, W. C., 1975, *Atlas for Objective Prism Spectra;* Bonner Spectral Atlas II., Ferd. Dümmler Verlag, Bonn.

Steinlin, U. W., 1968, *Zeitschrift für Astrophysik*, **69**, 276.

Upgren, A. R., 1962, *Astron. J.*, **67**, 37.

Woolley, R., Stewart, J. M., 1967, Mon. Not. R. Astr. Soc., 136, 329.

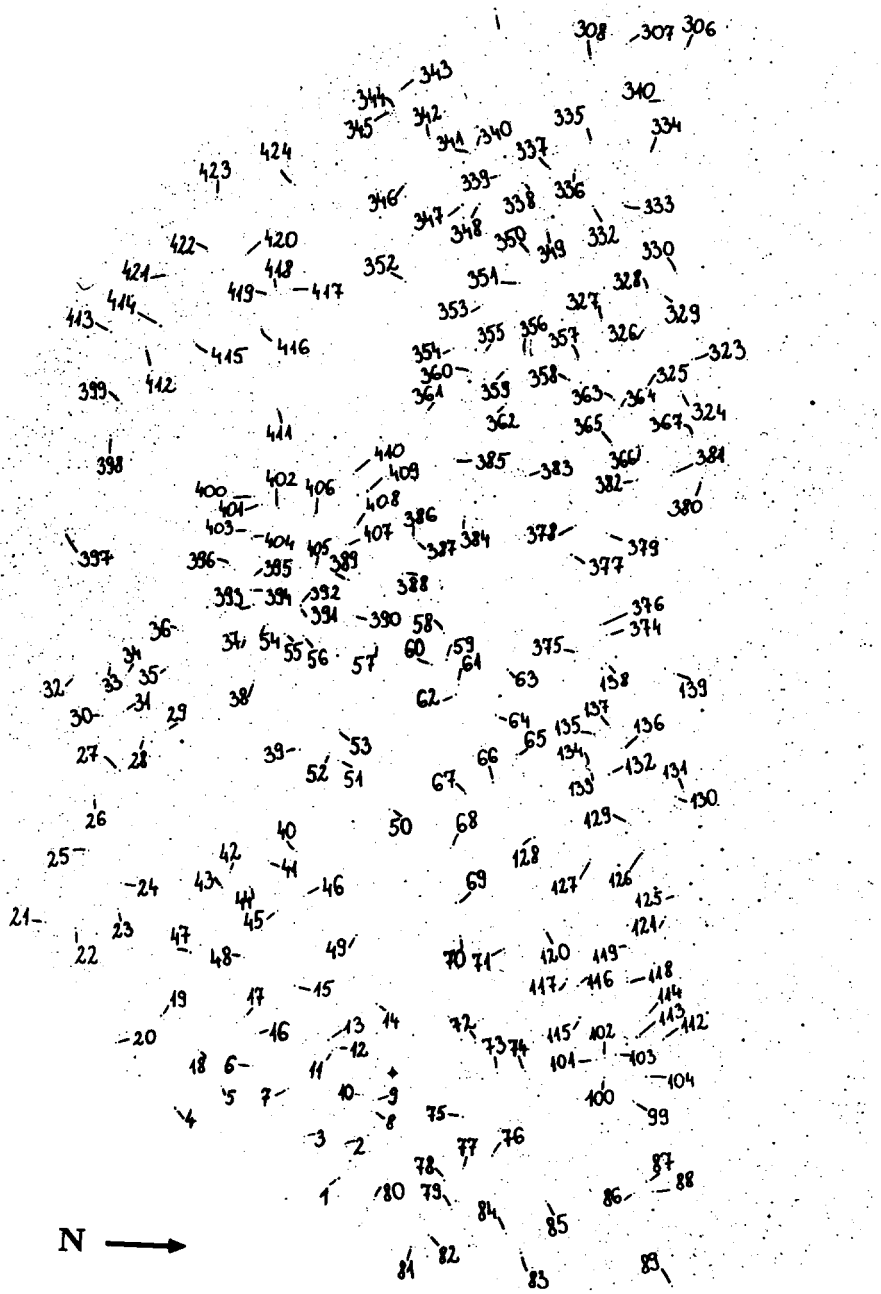

Finding chart of the survey stars

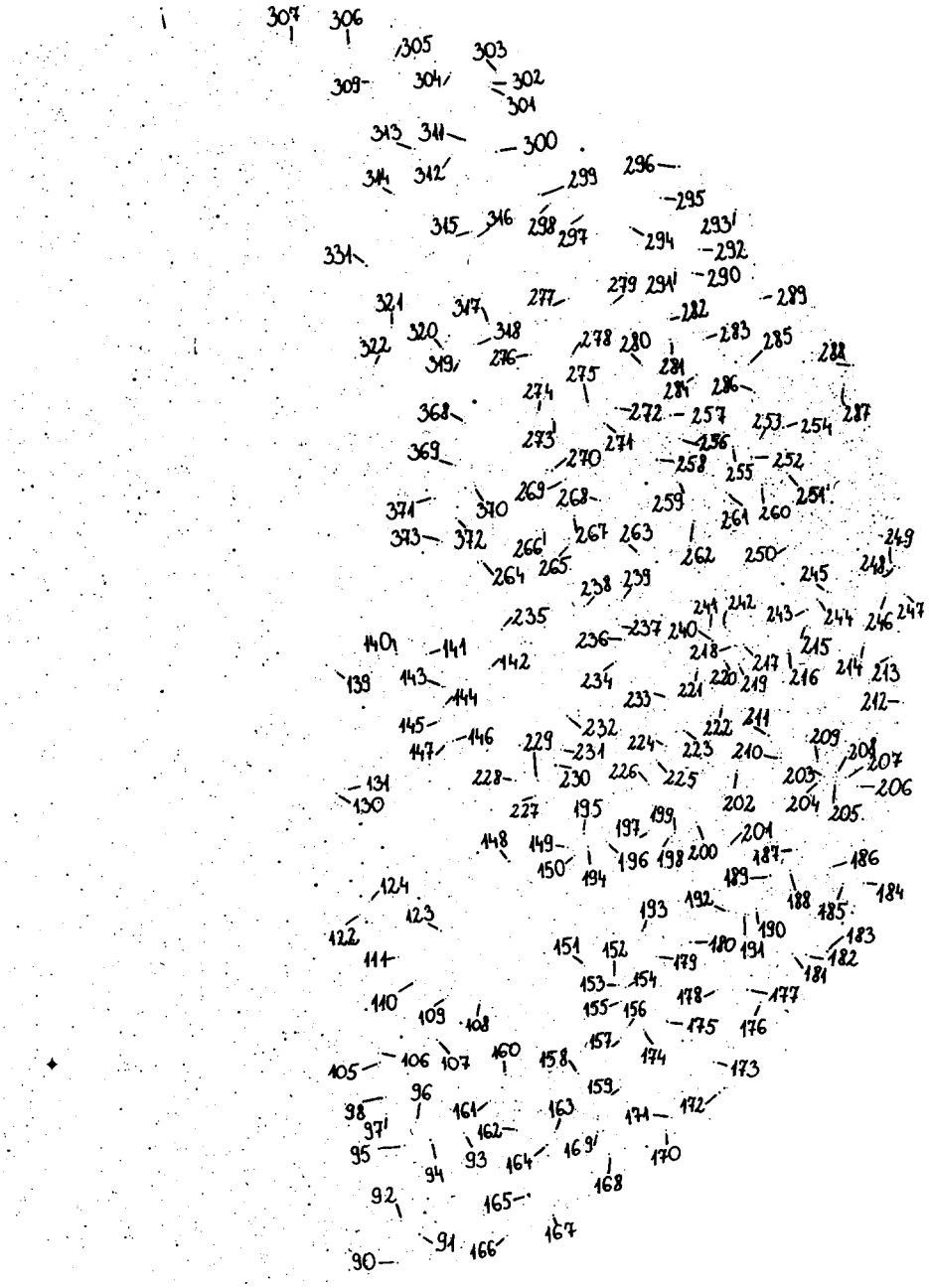

Finding chart of the survey stars

Table 6.

(Spectra and photometric data of survey stars)

No.	Sp.	V	B-V	U-B	G	G-R	U-G	remarks
1	G5 III	7.04	0.87	0.41	7.54	1.44	1.97	
2	K5:	11.34	1.62	1.74	12.59	2.59	3.35	
3	K2 III	10.03	1.39	1.48	10.83	2.01	3.31	
4	M5 III	10.43:	1.92:	1.39	11.87	3.24:	2.98:	
5	K5 III	9.78	1.63:	1.99:	10.70	2.48	3.97	
6	K2:	11.18	1.00	0.70	11.85	2.01	2.23	
7	K2 III	9.68	1.47	1.59	10.44	2.08	3.55	
8	G2	11.45	0.97	0.12	12.50	1.39:	1.15:	early
9	K0 III	11.29	1.18	0.77	12.06	2.09	2.35	
10	G2	11.40	0.92	0.04	11.91:	1.78:	1.57:	blend
11	M0 III	9.67	1.75	1.63	10.69	2.47	3.55	
12	G5:	11.75	0.77	0.01	12.22	1.55	1.45	
13	K5 III	8.01	1.58	2.05	8.92	2.26	4.01	
14	G8	9.72	0.78	0.35	10.06	1.27	1.99	
15	K0 III	9.56	1.15	1.02	10.13	1.83	2.82	
16	K2:	11.37	1.37	1.27	12.30	2.24	2.92	
17	K0 III	10.77	1.18	0.72	11.51	2.01	2.33	
18	G0	11.58	0.80	0.04	11.99	1.68	1.57	early
19	F8	9.74	0.53	0.10	9.84	1.34	1.74	
20	K5 III	11.07	1.56	1.61	11.95	2.49	3.51	early
21	K5:	11.52:	0.39:	0.66:	11.46	1.88:	2.44:	edge
22	G2	10.85	0.87	0.04	11.32	1.56:	1.56:	early
23	K5 III	9.63	1.74	2.02	10.60	2.61	4.04	
24	M0 III	10.67	1.78	1.82	11.56	2.53	3.91	
25	K2 III	10.95	1.41	1.37:	11.71	2.41:	3.24:	
26	K2	11.14	1.40	0.93	11.85	2.40	2.77	
27	K2 III	8.82	1.53	1.55	9.58	2.18	3.54	
28	M0 III	10.34	1.64	1.83	11.15	2.44	3.91	
29	M0:	10.89	1.74	2.10	11.93	2.70	4.06	
30	G8 III	11.19	1.07	0.61	11.73	1.85:	2.32	
31	M0 III	9.76	1.82	1.21	10.53	2.72	3.36	
32	K0:	11.00	1.16	0.50:	11.59	2.00:	2.21:	
33	K0 III	10.56	1.16	0.79	11.10	2.04	2.59	
34	K0 III	11.13	1.23	0.76	11.87	2.30:	2.41:	
35	K0	10.82	0.96	0.53	11.30	1.84	2.19	
36	K0 III	10.49	1.10	0.80	10.97	1.94	2.61	
37	K0 III	10.29	1.23	0.95	10.86	1.90	2.81	
38	G5:	11.33	0.77	-0.16:	11.74:	1.69:	1.31:	blend
39	K0 III	9.74	1.19	1.27	10.30	1.84	3.15	
40	M0 III	10.44	1.75	2.01	11.53	2.66	3.92	
41	G0:	11.01:	0.91:	0.30:	11.72:	1.75:	1.66:	early
42	G8	9.63	0.91	0.36	10.11	1.56	1.95	
43	K2 III	10.84	1.37	1.17	11.67	2.14	2.91	
44	G0	11.68	0.77	0.02	12.08	1.58	1.54	
45	G5:	11.09	0.86	0.41	11.60:	1.77:	1.95:	blend
46	K2 III	9.20	1.55	1.88	10.18	2.30	3.72	
47	K0 III	9.71	1.30	1.11	10.35	1.85	2.97	
48	K5	10.88	1.21	1.19	11.77	2.24	2.75	
49	G8	8.80	0.89	0.29	9.23	1.37	1.91	
50	K5 III	9.51	1.63	1.79	10.41	2.31	3.75	

Table 6.
(Continued)

No.	Sp.	V	B-V	U-B	G	G-R	U-G	remarks
51	K2 III	10.67	1.38	1.46	11.63	2.28	3.12	
52	K5	10.91	1.27	0.94	11.62	1.92	2.68	
53	M0 III	10.06	1.77	2.26	11.12	2.66	4.25	
54	K0 III	10.78	1.11	0.77	11.27	1.74	2.57	
55	K0 III	11.03	1.16	0.93	11.76	1.99	2.56	
56	M5 III	11.24	1.77	1.66	12.13	2.54	3.72	
57	F8	10.90	0.69	-0.22	11.26	1.34	1.24	
58	F8	10.94	0.76	-0.10	11.58	1.70:	1.15:	early
59	G0	11.20	0.68	-0.01	11.63	1.39	1.39	
60	G5	11.11	0.81	0.28	11.67	1.53	1.71	
61	F8	11.48	0.64	-0.09	12.06:	1.83:	1.13:	early
62	G0	11.34	0.78	-0.02	11.89	1.67	1.34	
63	G5	10.93	0.95	0.08	11.83:	1.95:	1.25:	early
64	G0:	11.68	0.95	-0.10	12.33:	1.99:	1.28:	blend
65	G0	11.14	0.53	-0.23	11.57	1.29:	1.02	
66	G8	8.92	0.79	0.27	9.38	1.38	1.78	
67	K5 III	9.20	1.79	1.98	10.24	2.51	3.96	
68	K2 III	10.22	1.40	1.78	11.11	2.19	3.57	
69	K2 III	10.02	1.20	1.02	10.83	1.93	2.62	
70	K0:	10.62	0.80	0.68	11.13:	1.60:	2.21:	
71	G0	10.68	0.67	0.23	11.23	1.56	1.55	
72	K5:	10.70	1.25	1.04	11.50	1.98	2.69	
73	K0 III	10.96	1.11	0.85	11.80	2.08	2.32	
74	K0 III	10.08	1.16	0.99	10.84	1.92	2.61	
75	K2 III	9.14	1.26	1.26	9.82	1.72	3.07	
76	G8 III	9.42	1.02	0.90	9.99	1.55	2.58	
77	K0 III	10.45	1.17	0.97	11.18	1.77	2.61	
78	G0	11.84	0.76	0.01	12.54	1.64	1.22	
79	K0 III	11.28	1.33	0.75	12.34	2.08	2.16	
80	K5 III	10.12	1.61	1.72	11.30	2.42	3.38	
81	K0 III	10.60	1.08	0.98	11.33	2.04	2.56	
82	G2	9.97	0.88	0.16	10.45	1.54	1.70	early
83	K0 III	8.75	1.10	1.30	9.35	1.74	3.08	
84	G5:	11.75	1.27	0.57:	12.57:	2.05:	2.14:	
85	M0 III	10.44	1.69	1.76	11.61	2.56	3.50	
86	K0 III	10.87	1.30	1.03	11.73	1.96	2.66	
87	G8 III	10.21	1.10	0.68	10.83	1.66	2.33	
88	K0 III	9.13	1.05	0.82	9.74	1.51	2.47	
89	K2 III	11.10	1.44	1.80	11.87	2.80:	3.75:	
90	K0 III	11.19	1.03	1.22	11.70	2.10:	3.01	
91	G5	8.85	0.73	0.34	9.16	1.29	1.96	
92	G5:	11.74	0.71	0.13	12.42:	1.79:	1.33:	blend
93	G0	9.84	0.68	0.30	10.19	1.21	1.83	early
94	F8	8.87	0.56	0.17	9.00	1.04	1.81	
95	G0	10.70	0.71	0.11	11.06	1.29	1.64	
96	K0 III	10.62	1.03	0.84	11.16	1.57	2.54	
97	K0 III	10.95	1.16	0.89	11.57	1.71	2.63	
98	M0	10.67	1.47	1.11	11.63	2.32	2.78	
99	G0	11.17	1.00	0.44	11.96:	1.79:	1.81:	blend
100	M0 III	10.80	1.68	1.71	12.02	2.65	3.38	

Table 6.
(Continued)

No.	Sp.	V	B-V	U-B	G	G-R	U-G	remarks
101	G8	10.84	0.75	0.38	11.35	1.33	1.83	
102	G0	11.20	0.60	0.20	11.59	1.18	1.63	
103	K2 III	9.60	1.22	1.38	10.30	1.73	3.17	
104	M0:	10.76	1.78	0.65:	12.09:	2.71:	2.12:	blend
105	K2 III	10.25	1.52	1.76	11.32	2.31	3.47	
106	K2 III	10.97	1.58	1.85	11.93	2.08	3.73	
107	K0	10.19	0.80	0.54	10.64	1.38	2.11	
108	G2	11.22	0.74	0.25	11.79	1.55	1.61	
109	F8:	11.94	0.64	-0.07	12.50	1.61	1.17	
110	K5	11.24	1.21	1.11	12.19	1.92	2.60	
111	K2 III	10.20	1.19	1.33	10.87	1.71	3.11	
112	K2 III	9.29	1.18	1.37	10.04	1.80	3.07	
113	K2 III	8.01	1.29	1.29	8.73	1.68	3.09	
114	K5	10.69	1.24	1.04	11.51	1.87	2.66	
115	K0 III	7.83	1.17	1.19	8.51	1.69	2.93	
116	F8	11.24	0.66	0.06	11.85	1.56	1.28	
117	K2 III	9.64	1.23	1.15	10.36	1.71	2.89	
118	F8:	12.08	0.57	-0.02	12.60:	1.30:	1.21:	
119	K2 III	11.03	1.19	1.27	11.92	1.91	2.82	
120	K0 III	11.17	1.28	0.74	12.22	2.07:	2.12	
121	F8	11.41	0.50	-0.03	11.83	0.95	1.25	
122	G5	11.22	0.82	0.19	11.83	1.52	1.56	
123	F8	9.78	0.55	-0.03	10.11	1.10	1.37	
124	K0 III	10.71	1.20	1.10	11.41	1.74	2.82	
125	G0	11.45	0.61	0.05	11.94	1.26	1.36	
126	K0 III	10.59	1.15	1.25	11.30	1.71	2.95	
127	K0 III	10.30	1.17	1.16	11.02	1.93	2.84	
128	K0 III	10.98	1.18	0.98	11.87	1.99	2.48	
129	G0:	11.96	0.56	-0.05:	12.36:	1.15:	1.29:	
130	M0 III	8.31	1.63	2.16	9.30	2.17	4.10	
131	G2	11.37	0.69	0.20	11.87	1.32	1.58	
132	K0 III	8.41	1.12	1.04	9.06	1.63	2.74	
133	G0	11.45	0.61	-0.22	11.90	1.46	1.08	
134	G2	10.99	0.82	0.04	11.60	1.75	1.39	
135	K0 III	8.96	1.19	0.82	9.68	1.72	2.47	
136	G0:	11.66	0.75	-0.16	12.40:	1.47:	0.97:	
137	F8	11.65	0.57	-0.08	12.37	1.65	0.94	
138	K5 III	8.76	1.49	1.76	9.63	2.05	3.65	
139	G8 III	10.59	0.97	0.60	11.20	1.65	2.15	
140	G2	8.90	0.73	-0.06	9.23	1.03	1.48	
141	K0 III	10.24	1.05	0.81	10.76	1.50	2.55	
142	K5 III	8.92	1.67	1.97	9.86	2.11	3.96	
143	K2 III	9.10	1.37	1.53	9.87	1.85	3.38	
144	F8	10.37	0.54	0.04	10.59	1.12	1.55	early
145	K2 III	10.63	1.21	1.35	11.43	1.76	3.02	
146	K2 III	10.18	1.49	1.60	10.90	1.91	3.61	
147	F8	11.69	0.49	-0.07	12.34	1.40	0.96	early
148	G8 III	7.80	0.96	0.84	8.32	1.42	2.51	
149	G5	11.20	0.67	0.29	11.54	0.98	1.83	
150	M5 III	10.95	1.74	1.07	12.16	2.55	2.70	

Table 6.
(Continued)

No.	Sp.	V	B-V	U-B	G	G-R	U-G	remarks
151	F8	12.35	0.29	0.01	12.53	1.22	1.37	
152	G8 III	9.64	1.03	0.70	10.06	1.34	2.51	
153	K0 III	10.86	1.19	0.97	11.65	1.74	2.58	
154	K5 III	10.00	1.50	1.75	10.80	1.98	3.71	
155	K5 III	10.55	1.73	1.96	11.32	2.01	4.16	
156	K2 III	11.90	1.31	1.10	12.67:	1.55:	2.84:	early
157	F8	12.33	0.38	0.02	12.69	0.79:	1.27	early
158	K0 III	10.76	1.20	1.09	11.35	1.55	2.92	
159	K0 III	11.56	1.22	0.43	12.10	1.44	2.22	
160	G5	9.72	0.64	0.30	10.03	1.11	1.85	
161	K0 III	10.67	1.16	1.22	11.33	1.69	2.97	
162	K0 III	11.13	1.09	1.01	11.76:	1.68:	2.70:	
163	G5	10.66	0.71	0.27	10.91	1.16	1.92	
164	G8 III	8.89	0.94	0.85	9.30	1.41	2.62	
165	K0 III	5.99	1.05	1.29:	6.51	1.72	3.10:	HR6590
166	M0 III	9.88	1.52	1.75	10.89	2.53	3.51	
167	G0	10.71	0.61	0.05	10.88	1.12	1.67	
168	K2 III	10.24	1.38	1.39	10.86	1.86	3.38	
169	G0	10.68	0.61	0.09	11.78:	1.75:	0.79:	early
170	K5 III	11.01	1.62	1.55	11.66	2.01	3.72	
171	G5	11.29	0.75	0.30	11.59	1.14	1.95	
172	K5 III	10.01	1.54	1.93	10.66	1.98	4.10	
173	K0 III	10.87	1.15	1.06	11.42	1.75	2.89	
174	K2 III	10.72	1.21	1.00	11.26	1.53	2.87	
175	K2 III	10.97	1.33	1.34	11.69:	1.70:	3.18:	
176	K0 III	10.46	1.16	1.20	10.80	1.34:	3.27	
177	G2	12.24	1.09	0.41	12.68:	1.47:	2.20:	
178	G0	11.96	0.54	0.21	12.26:	0.91:	1.67:	
179	G2	11.11	0.75	0.28	11.50:	0.83:	1.83:	
180	K0 III	8.61	1.22	1.27	9.19	1.35:	3.16	
181	G0	11.26	0.64	-0.01	11.45	1.05	1.60	early
182	G8 III	10.22	1.01	0.66	10.51	1.46	2.57	
183	G5	10.73	0.70	0.17	10.75	1.26	2.03	edge
184	K0 III	10.28	1.14	0.89:	10.36	1.41	3.15:	edge
185	K2 III	9.76	1.19	1.24	10.06	1.71	3.37	
186	K0 III	11.62	1.11	0.91	12.06	1.83	2.79	
187	F8	10.94	0.60	-0.06	10.90	0.88	1.75	early
188	G2	10.90	0.50	0.19	10.95	1.03	1.87	
189	F8	10.32	0.68	-0.09	10.45	1.11	1.61	
190	G8 III	11.35	0.90	0.65	11.83	1.74	2.28	
191	G8 III	11.74	1.22	0.56	12.33	1.72	2.32	
192	M5	10.87	1.57	1.57	12.14:	2.94:	3.09:	
193	G0	8.62	0.60	0.24	8.92	0.91	1.76	
194	M5 III	11.27	1.71	0.97	12.44	2.54	2.60	
195	G5	8.40	0.84	0.70	8.83	1.28	2.35	
196	K0 III	10.05	1.07	1.26	10.51	1.50	3.15	
197	K0 III	11.37	1.26	1.11	11.99	1.70	2.96	
198	K2 III	10.99	1.26	1.38	11.70	1.87	3.19	
199	M0 III	9.75	1.61	2.23	10.71	2.32	4.19	
200	K2 III	10.93	1.15	1.36	11.59	1.58	3.12	

Table 6.
(Continued)

No.	Sp.	V	B-V	U-B	G	G-R	U-G	remarks
201	G2:	11.97	0.53	0.26	12.29	1.33	1.71	
202	G0	11.10	0.61	0.17	11.33	1.18	1.75	
203	F8	11.45	0.42	0.11	11.51	1.04	1.71	
204	F8:	12.00	0.49	0.11	12.09	1.22:	1.73	
205	G0:	12.06	0.57	0.02	11.98	1.17	1.86	
206	G8 III	11.45	0.96	0.77	11.62	1.47	2.78	
207	G8	10.78	0.72	0.38:	10.75	1.13	2.35:	
208	K0 III	11.24	1.21	1.19	11.56	1.74	3.31	
209	K0 III	10.59	1.04	1.24	10.79	1.56	3.36	
210	K0 III	10.89	1.05	1.07	11.35	1.72	2.91	
211	G8	9.09	0.65	0.62	9.20	1.15	2.43	
212	K0 III	10.73	0.99	1.46:	10.71:	1.16:	3.79:	edge
213	K0 III	10.48	0.93	1.15	10.56	1.48	3.29	
214	G8 III	11.49	0.94	0.70	11.30:	1.10:	3.04:	
215	K0 III	10.01	1.03	0.95	10.22	1.48	3.00	
216	K0 III	10.48	0.99	1.12	10.87	1.68	2.99	
217	K2 III	11.15	1.19	1.20	11.78:	1.80:	3.00:	
218	F8:	12.08	0.44	0.18	12.18	1.65:	1.76	
219	G5	11.00	0.60	0.31	11.24	1.43:	1.90	
220	K0 III	10.51	0.99	1.20	10.91	1.49	3.08	
221	K0 III	11.05	1.17	1.06	11.63	1.65	2.88	
222	K5 III	10.90	1.43	1.97	11.66	2.20	3.95	
223	K2 III	8.77	1.21	1.67	9.31	1.60	3.65	
224	G0	11.41	0.51	-0.17	11.83	1.08	1.09	
225	G2:	11.83	0.61	0.04	12.05	0.91	1.61	
226	F8:	11.95	0.45	0.04	12.24	1.27	1.42	
227	K2 III	10.97	1.20	1.11	11.84	1.92	2.66	
228	M0 III	9.93	1.60	1.89	10.91	2.37	3.77	
229	G5	11.25	0.96	0.32	11.75	1.41	1.93	
230	K5 III	7.55	1.45	2.05	8.51	2.24	3.86	
231	K0 III	10.76	1.08	1.07	11.31	1.57	2.85	
232	K0 III	11.26	1.22	0.89	11.91	1.59	2.64	
233	M5 III	11.46	1.69	1.66	12.38	2.28	3.63	
234	G8 III	9.75	0.94	0.84	10.21	1.34	2.56	
235	K0 III	8.86	1.23	1.27	9.53	1.62	3.07	
236	K2 III	10.78	1.19	1.43	11.38	1.69	3.30	
237	G0	10.91	0.59	0.27	11.46	1.47	1.53	
238	G2	11.78	0.65	0.22	12.26	1.25	1.59	
239	G2	11.32	0.64	0.15	11.70	1.25	1.60	
240	K2 III	10.81	1.28	1.54	11.54	1.93	3.37	
241	K0 III	10.89	1.15	1.16	11.41	1.68	3.03	
242	G0	11.23	0.57	0.27	11.62	1.22	1.68	
243	M5 III	10.54	1.64	1.31	11.38	2.58	3.27	
244	K0 III	10.89	1.02	1.46	11.13	1.66	3.56	
245	K2 III	9.08	1.06	1.65	9.35	1.46	3.78	
246	K0 III	11.47	1.10	1.11	12.25:	2.30:	2.68:	
247	K0	9.71	1.09	1.18	-	-	-	edge
248	G8:	10.98	0.92	0.58	-	-	-	early
249	K0:	10.71	1.07	1.10	-	-	-	
250	K0 III	11.00	1.23	1.09	11.44	1.49	3.10	

Table 6.
(Continued)

No.	Sp.	V	B-V	U-B	G	G-R	U-G	remarks
251	G5	11.08	0.81	0.39	11.75	2.00	1.72	early
252	G5 III	9.52	0.83	0.46	9.70	1.17	2.31	
253	G5:	11.48	0.67	0.34	11.78:	1.34:	1.92:	
254	K0 III	10.85	1.05	0.96	11.36:	1.84:	2.73:	
255	G8 III	10.38	0.90	0.63	10.78	1.46	2.35	
256	K0 III	11.09	0.89	0.89	11.59	1.63	2.53	
257	G0	8.62	0.68	0.09	8.83	1.04	1.73	early
258	K5 III	7.73	1.51	2.06	8.62	2.28	3.99	
259	K0 III	11.31	1.05	1.12	11.81	1.60	2.93	
260	K5 III	9.82	1.56	2.06	10.43	2.19	4.31	
261	G0:	12.07	0.41	0.13	12.35	1.40	1.50	
262	F8:	11.84	0.33	0.20	12.02	0.93:	1.62	
263	M5 III	10.46	1.63	1.21	11.34	2.47	3.10	
264	K2 III	9.35	1.33	1.66	10.10	1.68	3.52	
265	K0 III	10.54	1.01	1.11	11.20	1.59	2.72	
266	F8:	12.08	0.50	0.06	12.52	1.23	1.33	
267	K0	10.50	0.78	0.53	10.83	1.19	2.21	
268	M0 III	9.81	1.70	2.19	10.66	2.21	4.33	
269	K0 III	10.33	1.02	0.97	10.88	1.66	2.68	
270	K2 III	7.85	1.24	1.83	8.52	1.61	3.73	
271	G0	10.57	0.65	0.10	10.73	1.11	1.77	
272	G0	8.27	0.66	0.23	8.56	1.00	1.80	
273	F8	11.40	0.67	-0.02	11.74	1.02	1.47	
274	G8 III	10.83	0.94	0.78	11.44	1.50	2.34	
275	K2 III	11.06	1.34	1.62	11.96	2.03	3.34	
276	G5:	11.86	0.79	0.05	12.43	1.40:	1.41	
277	K0 III	10.59	1.01	0.99	11.32	1.72	2.52	early
278	G5	11.41	0.84	0.29	11.89	1.27	1.83	
279	G2	9.96	0.72	0.30	10.39:	1.25:	1.79:	early
280	K0 III	11.18	1.19	1.08	11.85	1.74:	2.82	
281	K0 III	10.74	1.03	1.14	11.22:	0.73:	2.95:	
282	G5:	11.57	0.60	0.23	11.79:	0.81:	1.82:	
283	G2	11.20	0.69	0.06	11.29:	0.78:	1.83:	
284	K5 III	8.84	1.54	2.03	9.57	1.82	4.13	
285	K2 III	10.20	1.48	1.96	11.07:	2.09:	3.87:	
286	G8	9.96	0.68	0.36	10.32:	1.24:	1.90:	
287	K2	10.25	1.29	1.40	-	-	-	edge
288	K0:	13.21	1.00:	0.23:	-	-	-	edge
289	K0 III	10.20	1.03	0.86	11.26:	1.94:	2.05:	
290	K2 III	8.89	1.18	1.59	9.46	1.54	3.51	
291	K0 III	10.91	1.02	1.10	11.60:	1.73:	2.69:	
292	G5:	11.64	0.79	0.25	12.41:	1.48:	1.44:	
293	K0:	10.16	1.10	0.70	-	-	-	edge
294	K0 III	10.88	1.07	0.90	11.81:	1.63:	2.26:	
295	K0 III	8.71	1.12	1.17	9.38	1.55	2.87	
296	K5	7.45	1.66	2.52	-	-	-	edge
297	G5	10.56	0.67	0.31	10.92:	1.03:	1.83:	early
298	K0 III	11.37	1.03	0.90	12.33:	1.80:	2.19:	
299	G2	11.26	0.66	0.32	11.94:	1.34:	1.51:	
300	G8 III	8.40	0.89	0.79:	8.97:	1.23:	2.35:	

Table 6.
(Continued)

No.	Sp.	V	B-V	U-B	G	G-R	U-G	remarks
301	G2:	11.71	0.67	0.23	-	-	-	
302	G2:	11.52	0.61	0.15	-	-	-	
303	K2:	10.77	1.30	1.37:	-	-	-	edge
304	K5	11.08	1.82	2.30:	-	-	-	
305	K5	9.36	1.61	2.11	-	-	-	
306	K0	9.99	0.93	0.56	-	-	-	
307	K2	10.38	1.16	1.46	-	-	-	edge
308	K5 III	9.56	1.75	2.38	11.63:	3.15:	3.36:	
309	G2	11.38	0.86	0.19	12.70:	1.81:	0.89:	
310	K2 III	10.77	1.45	1.38	12.19:	2.55:	2.62:	
311	K5 III	8.95	1.47	2.00	10.07	1.93	3.65	
312	G0:	12.02	0.59	0.13	12.57:	1.06:	1.37:	
313	K2 III	9.89	1.35	1.19	10.78	1.87	2.86	
314	K0:	11.15	1.11	0.83	12.26:	1.87:	2.03:	
315	G2	11.22	0.65	0.22	11.67:	0.93:	1.62:	
316	G2:	11.61	0.72	0.09	12.04:	1.01:	1.55:	early
317	M0 III	10.36	1.70	2.15	11.56	2.45	3.93	
318	K5	11.07	1.11	1.07	11.89	1.82	2.60	
319	G5:	11.70	0.70	0.26	12.39:	1.44:	1.47:	
320	M5 III	11.48	1.59	1.83:	12.85	2.69	3.30:	
321	G8 III	10.19	0.99	0.85	10.77	1.50	2.49	
322	M0 III	11.11	1.72	1.88	12.47	2.51	3.47	
323	G0	11.32	0.77	0.06	11.91	1.55	1.39	
324	G8 III	11.57	0.86	0.55	12.12:	1.50:	2.06:	
325	M0:	11.87	1.80	0.86	13.52:	3.33:	2.07:	
326	G5	11.12	0.78	0.27	11.95:	1.84:	1.40:	
327	K2 III	10.85	1.35	1.47	11.92	2.20	3.00	
328	K5 III	10.38	1.41	1.77	11.36	2.13	3.48	
329	K5 III	10.16	1.59	2.03:	11.24	2.29	3.83:	
330	K5 III	11.32	1.60	1.69	12.55	2.42	3.29	
331	K5 III	7.25	1.56	2.34	8.14	2.12	4.35	
332	K0 III	9.99	1.05	1.20	10.48	1.61	3.03	
333	K0 III	11.01	1.17	0.97	11.64	1.51	2.72	
334	G0	10.83	0.85	0.40	11.76	1.51	1.50	early
335	K2:	10.97	1.00	0.63	12.12:	1.94:	1.67:	
336	K0	10.55	0.95	0.41	11.29	1.68	1.79	
337	K0 III	10.63	1.31	1.26	11.88:	2.30:	2.55:	
338	K2 III	9.62	1.24	1.43	10.46	1.95	3.10	
339	F8	11.32	0.57	0.03	12.12:	1.69:	0.99:	early
340	F8:	11.57	0.56	0.11	12.65:	1.87:	0.79:	
341	G0:	12.14	0.57	-0.25	13.26:	1.92:	0.34:	
342	G5:	11.61	0.85	-0.05	12.45:	1.80:	1.07:	
343	M5 III	9.57	1.63	1.26	10.85	2.71	2.76	
344	G5	11.41	1.12	0.57	12.69:	2.19:	1.57:	
345	G5	11.48	1.31	0.47	12.95:	2.36:	1.41:	
346	G8	10.89	0.84	0.23	11.75	1.66	1.38	
347	K0 III	7.78	1.07	0.96:	8.43	1.66	2.61:	
348	K2 III	8.82	1.30	0.85	9.65	1.84	2.48	
349	K0 III	11.21	1.21	0.82	11.78	1.46	2.64	
350	K0 III	11.36	1.04	0.45:	11.99:	1.25:	2.02:	

Table 6.
(Continued)

No.	Sp.	V	B-V	U-B	G	G-R	U-G	remarks
351	K0 III	9.99	1.07	0.86	10.65	1.72	2.48	
352	K0	9.65	1.09	0.58	10.19	1.71	2.29	
353	F8	11.85	0.57	-0.03	12.45	1.52	1.11	
354	K2 III	10.24	1.25	1.20	11.09	2.13	2.83	
355	K0	11.58	0.89	0.16	12.13	1.55	1.64	
356	F8	11.84	0.35	-0.07	12.19	1.20	1.15	
357	G5:	11.56	0.92	0.30	12.50:	2.06:	1.43:	blend
358	G2	8.28	0.90	0.43	8.81	1.45	1.98	
359	K0 III	9.87	1.20	0.99	10.66	1.93	2.60	
360	K2 III	10.79	1.28	1.24	11.67	2.19	2.87	
361	G5	11.34	1.02:	0.33:	12.15:	1.94:	1.68:	blend
362	G8 III	9.03	1.09	0.69	9.69	1.69	2.30	
363	G0 III	9.22	0.95	0.70	9.84	1.46	2.25	early
364	K2 III	10.48	1.28	1.27	11.37	1.96	2.89	
365	G5:	11.41	1.01:	0.40:	12.17:	1.98:	1.80:	
366	K2 III	10.07	1.17	1.46	10.91	1.95	3.08	
367	K2 III	10.69	1.39	1.82	11.65	2.24	3.54	
368	G5	11.18	0.76	0.13	11.89	1.45	1.34	
369	K5 III	10.55	1.57	1.74	11.47	2.30	3.63	
370	G2	11.22	0.62	0.16	11.62	1.23	1.58	
371	K0 III	9.63	1.05	1.07	10.12	1.46	2.88	
372	G5	10.21	0.66	0.39	10.52	1.12	1.96	
373	K0	11.07	0.77	0.47	11.63	1.40	1.90	
374	K0 III	9.82	1.20	1.07	10.55	2.01	2.76	
375	G8 III	11.06	1.22	0.52	11.97:	2.05:	1.96:	early
376	K2 III	9.43	1.44	1.50:	10.36	2.21	3.24:	
377	K2 III	6.92	1.31	1.58	7.67	2.04	3.41	
378	K0 III	9.82	1.02	0.60	10.37	1.62	2.25	
379	K2 III	9.80	1.30	1.70:	10.54	2.03	3.56:	
380	G5	11.61	0.90	0.25	12.29	1.62	1.63	
381	G8 III	10.91	1.00	0.69	11.60	1.80	2.20	
382	G5	11.08	0.85	0.16	11.72	1.50	1.52	early
383	G0	11.35	1.01	0.21	12.19:	1.91:	1.50:	blend
384	K5 III	9.18	1.54	1.59	9.95	2.01	3.58	
385	G5	11.20	1.40	-0.28	12.42:	1.77:	0.85:	blend
386	K0 III	10.97	1.39	0.99	11.83	2.13	2.68	
387	F8	11.89	0.49	-0.20	12.37	1.64:	0.98	
388	K0 III	10.23	1.05	0.79	10.92	1.96	2.35	
389	K5 III	8.66	1.76	2.02	9.72	2.49	3.97	
390	K0 III	11.43	1.13	0.75	12.07	1.78	2.42	
391	K0 III	10.08	1.15	0.77	10.76	1.97	2.42	
392	K5 III	10.37	1.53	1.46	11.23	2.35	3.34	
393	G5	8.94	0.70	-0.12	9.16	1.15	1.49	
394	K0 III	8.73	1.20	0.76	9.29	1.74	2.56	
395	K0 III	10.91	1.20	0.64	11.64	1.99	2.26	
396	K2 III	10.56	1.32	1.33	11.39	2.14	3.05	
397	K2 III	11.51:	1.45:	1.17	11.85	2.14:	3.46	
398	K2 III	9.92	1.30	1.27	11.45	2.97:	2.27	
399	K0 III	9.79	1.03	0.84	10.31	1.93	2.57	
400	K5 III	10.76	1.66	1.71	12.02	2.79	3.33	

Table 6.

(Continued)

No.	Sp.	V	B-V	U-B	G	G-R	U-G	remarks
401	K0 III	10.70	1.29	0.98	11.39	2.03	2.77	
402	G5	10.10	0.80	0.15	10.50	1.41	1.71	
403	K0:	11.62	1.19	0.19:	12.27:	1.94:	1.81:	
404	K0 III	10.89	1.32	0.71	11.61	2.15	2.44	
405	K5 III	10.29	1.57	1.81	11.12	2.35	3.81	
406	G0	10.93	0.62	-0.20	11.22	1.36	1.28	
407	K5 III	9.53	1.73	2.13	10.53	2.41	4.13	
408	K0 III	9.75	1.12	0.94	10.35	1.69	2.67	
409	K5 III	6.63	1.74	2.21	7.80	2.48	4.06	
410	K2	10.74	1.13	0.74	11.45	1.98	2.33	
411	G0:	11.84	0.57	-0.17	12.41:	1.73:	0.99:	blend
412	G0	11.35	0.54	0.05	11.96:	1.84:	1.18:	
413	G2	9.52	0.78	-0.18	9.90	1.51	1.33	early
414	K2 III	6.62	1.25	1.64	7.47	2.25	3.34	
415	G2	11.35	0.57	0.23	11.91	1.89	1.46	
416	K0	11.29	1.03	0.94	12.23:	2.30:	2.26:	
417	G8	11.16	1.04	0.74	11.99:	2.05:	2.15:	
418	K0	11.04	1.03	0.72	11.92	2.14	2.07	
419	F8	10.69	0.73	-0.27	12.44:	2.31:	-0.18:	early
420	K0 III	10.85	1.05	0.92	11.91	2.31	2.14	
421	K5:	11.21	1.55	0.65	12.23:	2.41:	2.25:	early
422	G2	11.55	0.64	0.12	12.30:	2.15:	1.20:	
423	G2:	11.49:	0.01:	0.12	11.88:	1.56:	1.07:	
424	K0 III	8.92	1.31	1.62	9.80	2.17	3.33	

Blend is remarked if the photographic image of the measured star is distorted by a neighbouring star.

Edge is remarked if the star is near the edge of the plate.

Early is remarked if the star was classified earlier than F8 in the previous paper (*Paparó* and *Balázs* 1982).

A colon beside the spectral type or figure denotes that the star was classified from one plate or the value was uncertain.